H-Band Multilayer Waveguide Incorporating a Locally Glide-Symmetric Electromagnetic Bandgap Structure

H-Band Multilayer Waveguide Incorporating a Locally Glide-Symmetric Electromagnetic Bandgap Structure

Jorge Martín-Villar, Martin Petek, *Member, IEEE*, Jorge A. Tobon Vasquez, Haojie Chang, *Member, IEEE*
Zhongxia Simon He, *Senior Member, IEEE* and Francesca Vipiana *Senior Member, IEEE*

***Abstract*—This letter presents an H-band (220-330 GHz) fully-metallic multilayer waveguide (MLW), that consists of five stacked metallic layers forming an air-filled groove. The waveguide is surrounded by a locally glide-symmetric holey electromagnetic bandgap (EBG) structure that prevents electric-field leakage across the interlayer gaps. A diamond-shaped unit cell is selected for the EBG due to its high effectiveness in suppressing leakage. To enable practical characterization, a well matched vertical transition is developed using a discretized stepped corner via a novel design process, crucial to achieve good impedance matching at high frequencies. The prototype exhibits a measured reflection coefficient lower than -10 dB in the entire H-band, and an average loss of the waveguide channel of 0.032 dB/mm.**

***Index Terms*—Electromagnetic modeling, Electromagnetic propagation, Periodic structures, Submillimeter wave devices, Waveguides.**

I. Introduction

The sub-THz band (100–300 GHz), particularly the H-band (220–330 GHz), is a key enabler for future high-capacity wireless communications. It is especially attractive for "last-mile" connectivity, backup links, and high-speed indoor communications, providing ultra-high-speed links exceeding 100 Gbps where fiber deployment is impractical [1].

Within the 6G vision, sub-THz frequencies are expected to support extreme data rates while enabling integrated communication, sensing, and imaging [2]. However, realizing components at these frequencies requires fabrication technologies capable of achieving tight tolerances while maintaining low loss and high power handling.

Manuscript received ; revised

This work has been partially supported by the EU GENIUS Project (GA:101072560), by the Sweden Vetenskaprådet project HI-CORE (2023-05184), and by Interreg CE MedWaveImage project (CE0200670). *(Corresponding author: Francesca Vipiana)*

Jorge Martin-Villar is with the Dept. of Electronics and Telecommunications, Politecnico di Torino, Torino, Italy, and also with Sinowave AB, Gothenburg, Sweden (e-mail: jorge_martin@polito.it).

Martin Petek and Francesca Vipiana are with the Dept. of Electronics and Telecommunications, Politecnico di Torino, Torino, Italy (e-mails: martin.petek@polito.it, francesca.vipiana@polito.it).

Haojie Chang is with the Dept. of Microtechnology and Nanoscience, Chalmers University of Technology, Gothenburg, Sweden (e-mail: haojie@chalmers.se).

Zhongxia Simon He is with the Beijing Institute of Technology, Zhuhai, China, and also with Sinowave AB, Gothenburg, Sweden (e-mails: zhongxia@bit.edu.cn, simon@sinowave.se).

Jorge A. Tobon Vasquez is with Wavision s.r.l, Torino, Italy (e-mail: jorge.tobon@wavision.it).

Hollow waveguides offer excellent low-loss and high-power performance because they are fully air-filled, but their fabrication involves complex and costly processes [3], [4]. Planar transmission lines and substrate-integrated waveguides are compact and low-cost but suffer from dielectric losses at sub-THz frequencies [3]. Gap waveguides (GWs) combine low losses with simplified, cost-effective fabrication by guiding electromagnetic waves between parallel plates without requiring continuous metallic contact [5]. A sub-THz ridge GW incorporating electromagnetic bandgap (EBG) pins was demonstrated in [6]. However, the polymer-based implementations of [6] may present limitations in high-power scenarios because of their relatively low thermal conductivity and higher thermal expansion coefficients.

To address these challenges, multilayer waveguide (MLW) technology represents an alternative manufacturing approach based on stacking thin metallic layers incorporating engineered electromagnetic periodic structures. This compact, air-filled, fully-metallic waveguide supports high power handling and can be fabricated using photochemical milling (PCM), a precise, cost-efficient method compatible with mass production. In [7], a five-layer MLW achieved a transmission coefficient better than -1 dB in the D-band (110–170 GHz), and [8] proposed slot array antennas in MLW technology working within 77–85 GHz. Recently, [9] presented waveguide antennas working at 92.5, 180 and 275 GHz with a relative bandwidth of 2.15%, using 0.6 mm-thick metal plates fabricated via laser cutting.

To the best of the authors' knowledge, this work demonstrates, for the first time, that MLW technology can be engineered to cover the entire 220–330 GHz H-band, corresponding to a relative bandwidth of 40%. The proposed waveguide employs a five-layer structure with diamond-shaped EBG unit cells placed near the groove edges to suppress leakage while maintaining compactness and proper impedance matching. Furthermore, a vertical transition, which is a key element for integration with other components, is designed through a novel methodology assuming a zero-gap condition between metallic layers, since conventional design approaches employed at lower frequencies cannot be directly applied in this frequency range.

II. Unit Cell Design

First, we design a periodic element used to suppress leakage of electromagnetic (EM) waves through the groove along the gaps among the metallic layers of the MLW, that would negatively affecting the transmission parameters [8]. Here, to avoid the field leakage, a locally glide-symmetric structure is designed. The term locally glide-symmetric refers to the fact that the structure exhibits glide symmetry when considering a pair of adjacent layers, even though the complete structure is not glide-symmetric. Specifically, following the insights from [7], a square holey structure is selected, as shown in Fig. 1(a). In the figure, g is the air gap between adjacent metallic layers, L is the hole square side, P is the cell period and r_i is the interior radius of the corners.

To design this unit cell, the following limitations of the manufacturing process must be taken into account. The thickness of the metallic layers is limited to $100\,\mu$m to avoid the tapering effects that thicker etched plates would exhibit at their edges. Furthermore, the minimum interior radius of the corners is $50\,\mu$m (i.e., half of the thickness of the metallic layers). Finally, the assumed maximum interlayer gap is $10\,\mu$m, following previous works [7], [8], [10].

The number of metallic layers is set to five, resulting from a trade-off: fewer layers reduce the number of gaps (hence the possible leakage) and the cost, but too few make it difficult to design a well-matched vertical transition, detailed in Sect. IV.

The stopband boundaries were evaluated with the CST ES, placing perfect electric conductor boundary conditions above and below the structure, for different values of P, L/P, r_i and g. The stopband is maximized while satisfying the manufacturing constraints. Accordingly, we select $P = 700\,\mu$m and $L = 500\,\mu$m, together with the minimum allowable corner radius, providing coverage over the entire H-band.

The complete dispersion diagram of the unit cell is shown in Fig. 1(b). It is evaluated in two different ways with excellent agreement: with CST ES and with the multimodal transfer matrix method (MMTMM) [11], [12]. The stopband covers the entire H-band in all the paths of the Brillouin zone, with the lower bound (at Γ) 216 GHz and the upper bound (at M) 357 GHz.

The dispersion diagram exhibits a glide symmetry-like behaviour: the mode pairing typical of glide symmetry is only partially observed, with pairs of modes coalescing at M but only two pairs at X [13]. This is because two adjacent plates are glide symmetric, even if the total structure is not. Hence, we refer to this property as local glide-symmetry. Four TEM modes (i.e., with zero cutoff frequency) are present, corresponding to the number of air gaps.

The MMTMM enables also the evaluation of the stopband attenuation in its normalized form, α/k_0, where α is the magnitude of the complex part of the transverse wave vector and k_0 is the free-space wavenumber. Figures 1(c) and (d) present the normalized attenuation. The grey region marks the minimum attenuation of any mode within the stopband within the H-band (i.e., the worst-case performance of the unit cell) along the x-axis ($\overline{\Gamma \mathrm{X}}$) with $0.28 \leq \alpha/k_0 \leq 0.78$, and at a $45°$ incidence ($\overline{\mathrm{M}\Gamma}$) with $0.25 \leq \alpha/k_0 \leq 0.47$. Hence, the best orientation of the unit cell is such that the electric field is incident along $\overline{\Gamma \mathrm{X}}$, as similarly found in [14] and [9].

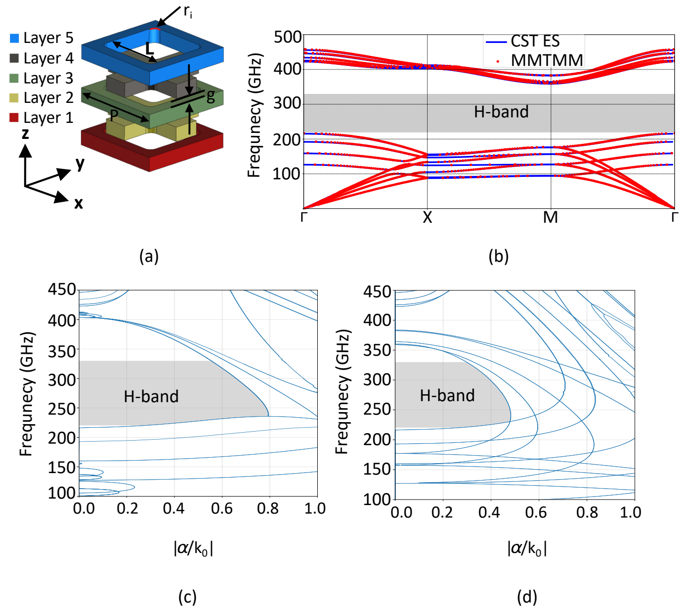

Fig. 1. Unit cell and simulation results. (a) Proposed unit cell, with $t = 100\,\mu$m, $g = 10\,\mu$m, $L = 500\,\mu$m, $P = 700\,\mu$m and $r_i = 50\,\mu$m. (b) Real part of the dispersion diagram: in blue solid lines CST ES results, red dotted lines MMTMM ones. (c) Normalized attenuation path along the $\overline{\Gamma \mathrm{X}}$ path. (d) Normalized attenuation path along the $\overline{\mathrm{M}\Gamma}$ path.

III. Multilayer Waveguide design

In this section, the designed MLW is analysed [see Fig. 2]. It consists of five silver-coated metallic layers, where layers 2–4 hold the groove and layers 1 and 5 enclose it at bottom and top. To prevent leakage, the unit cell, described in Sect. II, is placed along both sides of the groove in all layers; the waveguide is excited at ports 1 and 2, as marked in Fig. 2.

As discussed in Sect. II, the EBG confines better (i.e. the stopband attenuation is higher) if the wave is incident normally to the edge of the hole. As the wave propagating in the groove may be decomposed in two oblique TEM waves, we place the unit cell along the groove with a $45°$ tilt, as previously done with case of conventional glide-symmetric holey structures with one gap in [14]. Given that a 1-D periodic structure is targeted and the holes are rotated, the center-to-center spacing

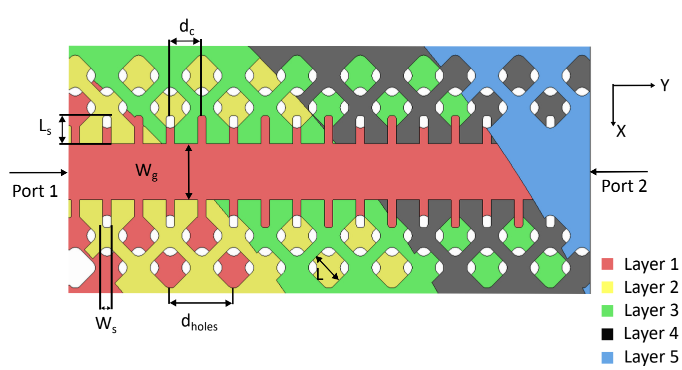

Fig. 2. MLW top view of the structure, cut to reveal each layer. The view includes the locations where ports are added for simulation purposes. The structure parameters are: $d_{holes} = 980\,\mu$m, $L = 500\,\mu$m, $W_{\mathrm{g}} = 864\,\mu$m, $L_{\mathrm{s}} = 400\,\mu$m, $W_{\mathrm{s}} = 125\,\mu$m, $d_{\mathrm{c}} = 490\,\mu$m.

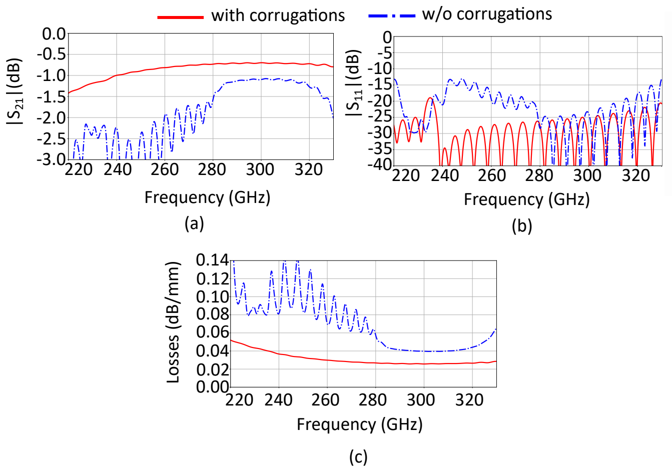

Fig. 3. MLW scattering parameters with and without corrugations. (a) Transmission parameters $|S_{21}|$. (b) Reflection parameters $|S_{11}|$. (c) Losses in dB/mm.

is defined as $d_{\text{holes}} = \sqrt{2}\,P$, as shown in Fig. 2. While the EBG structure suppresses leakage, transmission dips may still occur in its stopband due to modal conversion, Bragg reflection and other physical effects [15]. This issue is here resolved by placing corrugations in the three middle layers on both sides of the groove. These corrugations, reported in Fig. 2, have a periodicity $d_{\text{c}} = 490\,\mu$m, and dimensions $L_{\text{s}} = 400\,\mu$m and $W_{\text{s}} = 125\,\mu$m.

Figures 3(a) and (b) shows the obtained the MLW transmission and reflection coefficients, respectively, with and without corrugations, and it is evident that with corrugations both improve, especially at the band edges. To further clarify the benefits of the corrugations, we investigate the waveguide losses of the structure, in dB/mm, evaluated as follows:

$$\text{Loss} = \frac{10}{L}\log_{10}\left(\frac{(1-|S_{11}|^2)(1-|S_{22}|^2)}{|S_{21}|^2\,|S_{12}|^2}\right)^{1/2} \quad (1)$$

where L is the length of the waveguide channel in mm. Equation (1) extends the expression proposed in [16] by averaging the reflection and transmission parameters, thus accounting for asymmetric matching at the two ports, non-reciprocal behaviour, and measurement inaccuracies. These losses are reported in Fig. 3(c): it can be observed that the corrugations reduce them across the entire band. The average losses with corrugations are $0.033\,$dB/mm while, without them, they increase up to $0.082\,$dB/mm.

Furthermore, we may note the increase of losses at the upper and lower boundaries of the band, which are more prominent if no corrugations are used. We attribute this effect to the increased leakage caused by the lower stopband attenuation of the unit cell, shown in Fig. 1(c) and (d).

IV. Vertical Transition

The next step is the design of a vertical transition, needed because it is not practical to attach a flange to the sides of the horizontal configuration described in Sect. III. First, we design a curved bend with a standard WR3 metallic waveguide. Then, we discretize the curve using the available layers of the designed MLW. In the discretized version, the height of the waveguide depends directly on the number of layers, since the thickness of the plates is fixed. On contrary the width remains as the standard width of WR3.

In previous works utilizing the MLW technology [7], [8], the vertical transition was designed by assuming the same maximum permissible interlayer gap as it is assumed in design of the horizontal section of the waveguide. However, in this work, due to the much higher frequency than in [7], [8], this design procedure fails to provide sufficient matching when a prototype is manufactured. This is because with four gaps, the height of the structure is increased by $40\,\mu$m, i.e., by about 13%, creating the issue of which gap value should be selected. We found that an appropriate value is $0\,\mu$m, justified by the fact that the vertical transition is surrounded by the flange screws and thus tightly pressed together. This is further corroborated by previous studies on metallic contacts [17, Fig. 6(b)], which note that contact is ensured in the vicinity of the screw, while gaps may form at increasing distances from it.

Next, we provide design guidelines on how to choose the number of layers. With many layers, we may construct a very smooth vertical transition and thus trivialize the impedance matching. However, using too many layers increases the assembly complexity and the prototype cost, as manufacturing is done by arranging multiple waveguides on A4 sheets and fewer waveguides can be produced per sheet (e.g., ten with a four-layer design versus six with a six-layer one). Therefore, we aim to ensure a proper impedance matching while minimizing the number of layers. This is especially important in systems with several vertical transitions on different layers [8], where each added layer multiplies the additional cost by the number of all transitions.

To determine the number of needed layers, we perform a simulation with different numbers as shown in Fig. 4. The results indicate that a structure with only four layers (two inner layers) does not provide adequate matching in the H-band, while, with an additional layer (i.e. three inner layers), a significantly improved matching can be obtained, with the reflection coefficient of at least $-15\,$dB throughout the entire frequency range. Using six layers (four inner layers) enables matching the structure below $-20\,$dB. Here, we choose five layers as it provides a good balance between the performance of the vertical transition and its cost. The final values for each layer are $S_1 = 0.07\,$mm, $S_2 = 0.09\,$mm and $S_3 = 0.226\,$mm.

While the obtained vertical transition is designed for a zero gap, we nevertheless add surrounding structures to suppress any possible leakage in the event of a small gap appearing. The EBG structure is placed surrounding the waveguide ends, but it can be challenging to place it sufficiently close to the vertical transition. Therefore, slots are placed in the middle three layers, as seen for layers 2 and 3 in Fig. 5(a) and (b). They are placed as close to the waveguide channel and extend along the waveguide width as long as possible, considering that the distance between two etched holes (G_{L} and G_{os} in the figures) must be at least $100\,\mu$m in the PCM manufacturing process, from which we obtain the width w_{bs} and length L_{bs} of the slots.

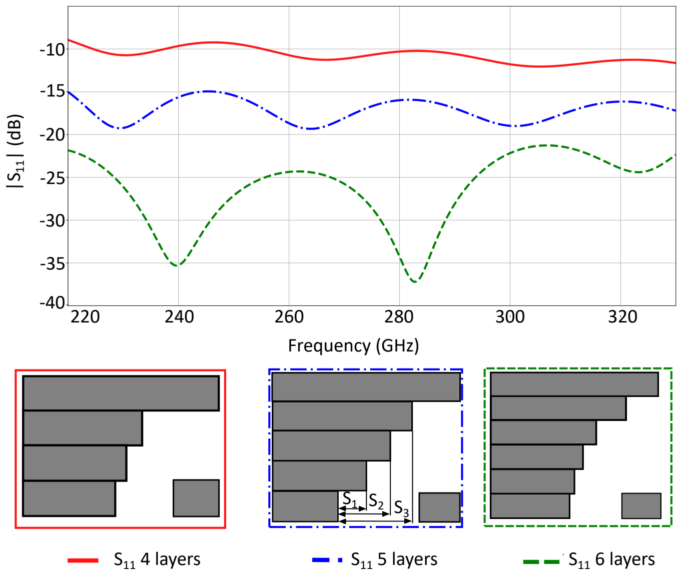

Fig. 4. Reflection coefficient at the vertical transition port using different numbers of layers. The thickness of the layers are fixed to $100\,\mu$m, and therefore the height of the waveguide is dependent on the number of layers.

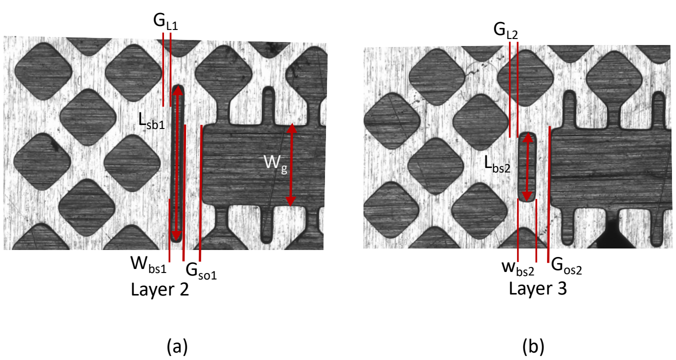

Fig. 5. Optical microscope image of the vertical transition. (a) layer 2 with slot dimensions $L_{\mathrm{bs1}} = 1720\,\mu$m, $w_{\mathrm{bs1}} = 125\,\mu$m, $G_{\mathrm{os1}} = 210\,\mu$m, $G_{L1} = 113\,\mu$m, $W_g = 864\,\mu$m. (b) layer 3 with slot dimensions $L_{\mathrm{bs2}} = 761\,\mu$m, $w_{\mathrm{bs2}} = 189\,\mu$m, $G_{\mathrm{os2}} = 165\,\mu$m, $G_{\mathrm{L2}} = 103\,\mu$m.

V. Prototype and Experimental Results

In this section, the prototype and its measurements are presented and compared to simulations. The different metallic layers of the manufactured prototype are shown in Fig. 6, while, in Figs. 5(a) and (b), the prototype details are presented under a microscope. A visual inspection indicates a remarkably high level of accuracy of the manufacturing process, indicated by a lack of obvious visual deformities in the hole shapes.

The measurements are performed with a Keysight N5242B VNA and WR3.4 (220–330 GHz) Virginia Diodes extenders driven by an N5261A Millimeter-Wave Controller. The measurement setup is shown as an inset in Fig. 7(a).

The magnitude of the measured scattering parameters, together with the simulated ones, and the losses for $g = 0\,\mu$m and $g = 5\,\mu$m, are shown in Fig. 7. In Fig. 7(a), we can observe that the measured transmission parameters lie between the two simulated gaps.

Then, both the measured $|S_{11}|$ and $|S_{22}|$, depicted in Fig. 7(b), are lower than $-10\,$dB throughout the band, and

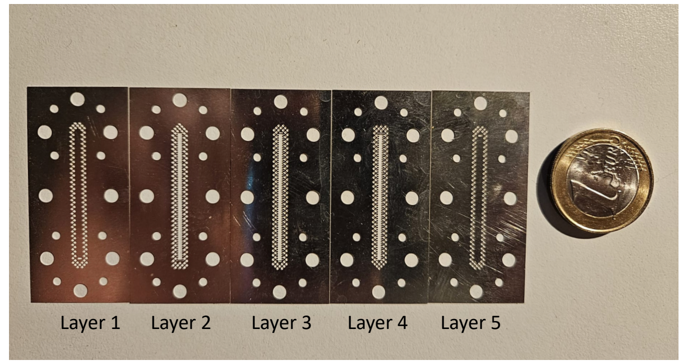

Fig. 6. Manufactured five-layer silver-plated MLW

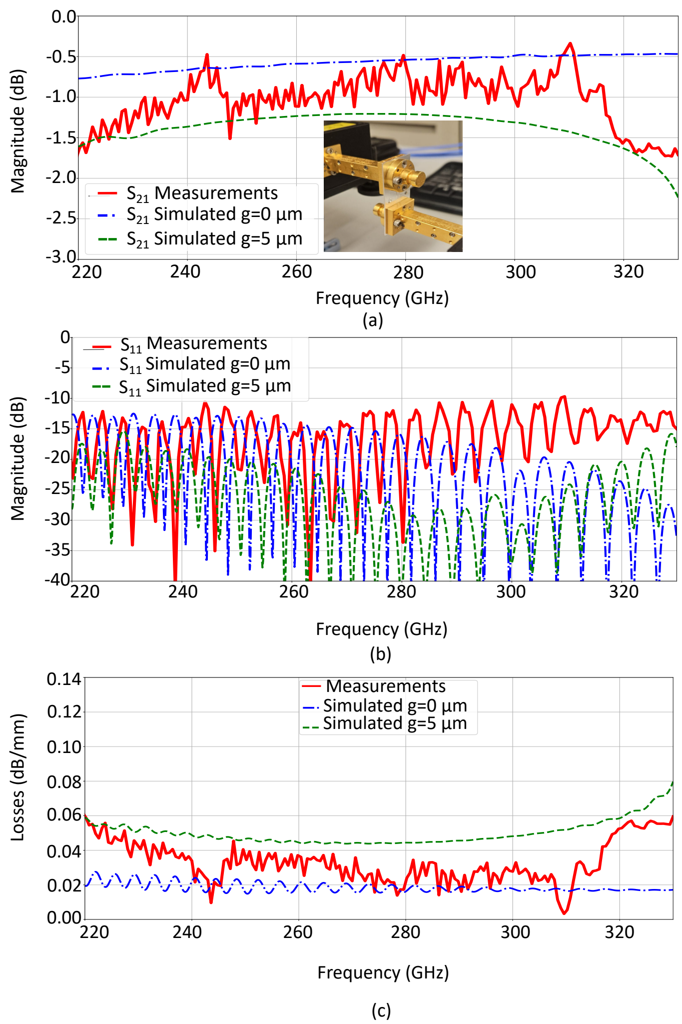

Fig. 7. Comparison between simulated and measured scattering parameters. (a) Transmission parameters. (b) Reflection parameters. (c) Losses of the waveguide channel in dB/mm.

they are in line with the simulated results, in particular with the case of $g = 0\,\mu$m. Finally, the losses, evaluated using (1), are reported in Fig. 7(c), and

are bound within the simulations of the two gaps. Hence, we may conclude that the manufacturing inaccuracies do not create gaps which cumulatively exceed the effect of a uniform $5\,\mu$m gap. The average of the measured losses within the entire

TABLE I
WAVEGUIDE MANUFACTURING PROCESSES AND LOSSES.

Ref.	Manufacturing	Coating	Freq. (GHz)	Losses (dB/mm)
[18]	CNC machining	Gold	220-330	0.021
[19]	DRIE	Gold	220-325	0.039
[20]	DRIE	No	260-400	0.005
[18]	SU-8	Silver	220-325	0.030
[21]	SU-8	Silver+Gold	220-325	0.134
[22]	SLM	Copper	220-325	0.120
This work	MLW-PCM	Silver	220–330	0.032

band is 0.032 dB/mm.

Finally, we compare our results with those of other waveguide technologies in Table I. The represented manufacturing techniques are well-established CNC machining [18], deep reactive ion etching (DRIE) for silicon-based waveguides [19], [20], SU-8 (polymer) micromachining [18], [21], and selective laser melting (SLM) [22], a 3D printing method for fully metallic structures. Notably, [20] employs no coating, as the waveguide is entirely constructed in silicon, while in [21] the thickness of the gold plating is lower than its penetration depth and hence the current partially flows in the lower silver layer. The MLW-PCM is among the lower loss waveguide technologies. Considering the fully-metallic constructions, its losses are notably lower than the SLM [22], and while CNC-manufactured waveguides report lower losses, the PCM offers the advantage of cost-effective mass production. When compared to non fully-metallic alternatives, its losses are comparable with the best-performing SU-8 waveguides [18]. Though DRIE may yield even lower losses [20], it lacks the benefits of a fully-metallic structure. Hence, the proposed MLW-PCM is a competitive alternative in the H-band.

VI. CONCLUSION AND PERSPECTIVES

In this work, we demonstrated the applicability of PCM-MLW technology to the H-band through the design, fabrication, and experimental characterization of a multi-layer waveguide covering the entire 220–330 GHz frequency range. The structure was created using five fully metallic layers stacked on top of each other to form a waveguide channel. Possible leakage in the structure was mitigated by the inclusion of periodic elements, designed to effectively reduce leakage for a maximum gap between the layers of up to 10 μm. We also proposed a modified design procedure for the vertical transition, required for an efficient matching of the structure to a rectangular waveguide. We manufactured and measured a prototype, obtaining a matching lower than -10 dB with average losses of 0.032 dB/mm. Through simulations, we estimated that the cumulative effect of leakage is lower than in a structure possessing a gap of 5 μm.

This work enables designs of highly-efficient antennas and antenna components in the H-band, which will be considered in a future work.

REFERENCES

[1] S. Koenig, D. Lopez-Diaz, J. Antes, F. Boes, R. Henneberger, A. Leuther, A. Tessmann, R. Schmogrow, D. Hillerkuss, R. Palmer, T. Zwick, C. Koos, W. Freude, O. Ambacher, J. Leuthold, and I. Kallfass, "Wireless sub-THz communication system with high data rate," *Nature Photon.*, vol. 7, pp. 977–981, 2013.

[2] Yang, Ping and Xiao, Yue and Xiao, Ming and Li, Shaoqian, "6G Wireless Communications: Vision and Potential Techniques," *IEEE Netw.*, vol. 33, no. 4, pp. 70–75, 2019.

[3] K. Wu, M. Bozzi, and N. J. G. Fonseca, "Substrate Integrated Transmission Lines: Review and Applications," *IEEE J. Microw.*, vol. 1, no. 1, pp. 345–363, 2021.

[4] H. Meng, Y. Chen, and W. Dou, "Design and Fabrication of W-Band Waveguide Slotted Array Antenna Based on Milling Process," *Int. J. Antennas Propag.*, vol. 2020, pp. 1–6, Feb. 2020.

[5] P.-S. Kildal, E. Alfonso, A. Valero-Nogueira, and E. Rajo-Iglesias, "Local Metamaterial-Based Waveguides in Gaps Between Parallel Metal Plates," *IEEE Antennas Wireless Propag. Lett.*, vol. 8, pp. 84–87, 2009.

[6] S. Farjana, A. U. Zaman, P. Lundgren, and P. Enoksson, "Micromachined Wideband Ridge Gap Waveguide Power Divider at 220–325 GHz," *IEEE Access*, vol. 10, pp. 27 432–27 439, 2022.

[7] A. Vosoogh, H. Zirath, and Z. S. He, "Novel Air-Filled Waveguide Transmission Line Based on Multilayer Thin Metal Plates," *IEEE Trans. Terahertz Sci. Technol.*, vol. 9, no. 3, pp. 282–290, 2019.

[8] C. Jin, J. Chen, B. Zhang, L. Kong, S. An, Z. S. He, and J. Liu, "Low-Cost mmWave Metallic Waveguide Based on Multilayer Integrated Vertical-EBG Structure and its Application to Slot Array Antenna Design," *IEEE Trans. Antennas Propag.*, vol. 70, no. 3, pp. 2205–2213, 2022.

[9] S. Garcia-Martinez, A. Tamayo-Dominguez, and P. Sanchez-Olivares, "Sub-Terahertz Waveguide Antennas Based on Contactless Thin Metal Sheets," in *Proc. 19th Eur. Conf. Antennas Propag. (EuCAP)*. European Association on Antennas and Propagation (EurAAP), 2025.

[10] W. Tan, Y. He, H. Luo, G. Zhao, and H. Sun, "Low-Cost Gap Waveguide Technology Using Shallow Grooves and Glide-Symmetric Semicircular-Holes EBG Structures," *IEEE Antennas Wireless Propag. Lett.*, vol. 22, no. 12, pp. 2901–2905, 2023.

[11] F. Mesa, G. Valerio, R. Rodríguez-Berral, and O. Quevedo-Teruel, "Simulation-Assisted Efficient Computation of the Dispersion Diagram of Periodic Structures: A comprehensive overview with applications to filters, leaky-wave antennas and metasurfaces," *IEEE Antennas Propag. Mag.*, vol. 63, no. 5, pp. 33–45, 2021.

[12] F. Giusti, Q. Chen, F. Mesa, M. Albani, and O. Quevedo-Teruel, "Efficient Bloch Analysis of General Periodic Structures With a Linearized Multimodal Transfer-Matrix Approach," *IEEE Trans. Antennas Propag.*, vol. 70, no. 7, pp. 5555–5562, 2022.

[13] O. Quevedo-Teruel, Q. Chen, F. Mesa, N. J. G. Fonseca, and G. Valerio, "On the Benefits of Glide Symmetries for Microwave Devices," *IEEE J. Microw.*, vol. 1, no. 1, pp. 457–469, 2021.

[14] Q. Chen, F. Mesa, X. Yin, and O. Quevedo-Teruel, "Accurate Characterization and Design Guidelines of Glide-Symmetric Holey EBG," *IEEE Trans. Microw. Theory Techn.*, vol. 68, no. 12, pp. 4984–4994, 2020.

[15] M. Chen, O. Zetterstrom, F. Mesa, and O. Quevedo-Teruel, "Spurious Transmission Dips in Waveguides Implemented with Glide-Symmetric Holey EBG," in *2025 19th Eur. Conf. Antennas Propag. (EuCAP)*, 2025, pp. 1–4.

[16] E. Rajo-Iglesias, M. Ferrando-Rocher, and A. U. Zaman, "Gap Waveguide Technology for Millimeter-Wave Antenna Systems," *IEEE Commun. Mag.*, vol. 56, no. 7, pp. 14–20, 2018.

[17] H. H. Gould and B. B. Mikic, "Areas of Contact and Pressure Distribution in Bolted Joints," June 1970, prepared for NASA Marshall Space Flight Center under Contract NAS 8-24867.

[18] X. Shang, M. Ke, Y. Wang, and M. J. Lancaster, "WR-3 Band Waveguides and Filters Fabricated Using SU8 Photoresist Micromachining Technology," *IEEE Trans. Terahertz Sci. Technol.*, vol. 2, no. 6, pp. 629–637, 2012.

[19] B. Beuerle, J. Campion, U. Shah, and J. Oberhammer, "A Very Low Loss 220–325 GHz Silicon Micromachined Waveguide Technology," *IEEE Trans. Terahertz Sci. Technol.*, vol. 8, no. 2, pp. 248–250, 2018.

[20] W. Gao, X. Yu, M. Fujita, T. Nagatsuma, C. Fumeaux, and W. Withayachumnankul, "Effective-medium-cladded dielectric waveguides for terahertz waves," *Opt. Express*, vol. 27, no. 26, pp. 38 721–38 734, Dec 2019.

[21] T. Skaik, Y. Wang, M. Ke, S. Qian, and M. Lancaster, "A micromachined WR-3 waveguide with embedded bends for direct flange connections," in *Proc. 40th Eur. Microw. Conf.*, 2010, pp. 1225–1228.

[22] B. Zhang and H. Zirath, "Metallic 3-D Printed Rectangular Waveguides for Millimeter-Wave Applications," *IEEE Trans. Compon., Packag., Manuf. Technol.*, vol. 6, no. 5, pp. 796–804, 2016.